AIAA JOURNAL
Vol. 44, No. 10, October 2006

Airfoil Shape Optimization Using a Nonuniform Rational B-Splines Parameterization Under Thickness Constraint

Simon Painchaud-Ouellet,* Christophe Tribes,† Jean-Yves Trépanier,‡ and Dominique Pelletier§
École Polytechnique de Montréal, Montréal, Québec H3C 3A7, Canada

DOI: 10.2514/1.15117

Results for 2-D airfoil shape optimization in transonic regime are presented. Airfoil shapes are represented by nonuniform rational B-splines with appropriate regularity properties. A Navier–Stokes flow solver is used to compute the flow field and to obtain aerodynamic coefficients. A design of experiment is conducted to select the most sensitive design variables among the nonuniform rational B-splines parameters to reduce their number in the final optimization process. Single-point and multipoint formulations of the optimization problem are proposed and compared. The nonuniform rational B-splines parameterization guarantees smooth optimized airfoils. The multipoint optimization formulation combined with the nonuniform rational B-splines parameterization leads to airfoils with good performance over a specified Mach range.

I. Introduction

AIRFOIL shape optimization using computational fluid dynamics (CFD) has received much attention in recent years. Improved access to powerful computers, the development of reliable optimization techniques and the broader accessibility to accurate and fast CFD codes have allowed aerodynamicists to push forward the development of new airfoils. In this quest, transonic airfoils constitute the focus of many studies because most commercial aircraft operate in this regime.

There are many ways to formulate an aerodynamic optimization problem; one possible way is the so-called *target* C_p formulation (a review of the numerous inverse methods for airfoil and wing design is given in Lores [1]), where the design engineer provides a target pressure distribution, and the optimizer is in charge of contouring the airfoil shape so as to force the pressure distribution to conform to the target distribution. This formulation works well but relies heavily on the expertise of the designer in transonic aerodynamics to define target C_p curves that are physically relevant, and whose corresponding airfoils will indeed provide good aerodynamic performance. In particular, the relation between a target C_p curve and the airfoil drag coefficient is far from obvious and only an experienced designer will possess the knowledge to successfully exploit this type of relation. Therefore, even though this formulation has been widely used in industry, its reliance on the engineer's experience makes it delicate to incorporate in a fully automated design procedure.

A second approach to the problem is the *drag reduction* formulation, which works directly on reducing the drag of the airfoil. In this case, the objective is to obtain the airfoil that minimizes drag (C_d) for a given lift (C_l^*) at a specified flight condition, that is, a given Mach number (M_∞) and Reynolds number (Re). However, several problems have been reported with this formulation: unrealistic airfoils, "bumpy" airfoils, and airfoils with poor off-design performance were obtained [2–4]. Based on these works, it appears that the drag reduction formulation can be even more difficult to use than the target C_p formulation. However, because of its great design potential, much effort has been expended to overcome the difficulties of the drag reduction method.

One of the main problems encountered in transonic drag minimization is that the optimal airfoils show very good performance at the design operating Mach number, but behave poorly as soon as flight conditions differ from the design operating point. This behavior, also referred to as localized optimization, corresponds to airfoils with bumps on the upper surface that reduce the strength of the shock wave for a given Mach number. Although helpful at the design point, these bumps are detrimental at any other flight condition.

The main objective of the present work is to determine if a more global geometric parameterization of the airfoils will avoid local minima encountered in previous studies. Basically, we want to assess the suitability of nonuniform rational B-splines (NURBS) for aerodynamic design optimization. One advantage of NURBS, over other parameterization techniques, is its seamless integration with standard CAD systems. Also, the NURBS representation, with the small number of control points it needs to define an airfoil, limits the occurrence of local bumps. Indeed, each control point has a more global influence on the definition of the geometry. As a second objective, we will investigate the differences between optimizing for a single Mach number (single-point formulation) and for a set of Mach numbers (multipoint formulation).

Optimizations are conducted with a transonic airfoil as an initial design point. A thickness constraint is added to account for the volume requirements of the wing box structure and fuel. Because the objective is to minimize the drag of the airfoil, a Navier–Stokes flow solver is used to accurately compute the viscous and compressible contributions to the drag of the airfoil.

II. Aerodynamics in Transonic Regime

An airfoil enters the transonic regime when local supersonic regions appear on the suction side of the airfoil. The Mach number for which this phenomenon occurs is referred to as the critical Mach number (M_{cr}), and its value is usually around $M_{cr} \approx 0.7$. At Mach numbers above the critical Mach number, a shock forms on the

Presented as Paper 1095 at the 42nd AIAA Aerospace Sciences Meeting and Exhibit, Reno, Nevada, 5–8 January 2004; received 16 December 2004; revision received 24 April 2006; accepted for publication 2 June 2006.

*Graduate Student, 2900, boulevard Édouard-Montpetit; currently with Biothermica Inc., Montreal, Canada; simon.painchaud-ouellet@polymtl.ca.

†Research Associate, 2900, boulevard Édouard-Montpetit; christophe.tribes@polymtl.ca.

‡Professor, 2900, boulevard Édouard-Montpetit; jean-yves.trepanier@polymtl.ca. Senior Member AIAA.

§Professor, Canada Research Chair, École Polytechnique de Montréal, 2900, boulevard Édouard-Montpetit; dominique.pelletier@polymtl.ca. Associate Fellow AIAA .

suction side of the airfoil and this significantly increases the drag of the airfoil for two reasons. Firstly, the total pressure loss across the shock causes *wave drag*; second, as M_∞ increases, the shock becomes strong enough to cause boundary layer separation at the foot of the shock. Flow separation causes significant increases of the total drag. This phenomenon is known as *drag divergence* [5]. Aircraft operating in the transonic regime are usually designed to fly at Mach numbers below that at which drag divergence occurs.

III. Localized Optimization

Recent work by Huyse et al. [3] discusses drag reduction for a NACA0012 airfoil in transonic flow. The airfoil was parameterized with splines using 23 control points and an Euler CFD code was used to obtain flow solutions. The main objective was to design airfoils with good performance over a given Mach range. The emphasis was placed on the formulation of the optimization problem.

The most obvious approach is the *single-point* formulation, where drag is reduced at constant lift for a specified flight condition. Huyse et al. [3] observed that the optimizer takes advantage of the flow field condition and reduces the drag by introducing a bump at the foot of the shock on the suction side. Because the shock position changes with M_∞, the bump becomes totally ineffective as M_∞ changes. Hence, single-point optimization leads to airfoils with poor off-design performance. This type of localized optimization associated with bumps had also been reported by Drela [2]. Figure 1 shows Huyse's results for the single-point optimization.

In practice, aircraft are expected to exhibit good performance over a reasonable range of Mach numbers. Huyse et al. [3] concluded that the single-point approach could not yield adequate airfoils and opted to investigate a multipoint approach in which every airfoil generated by the optimizer is evaluated at k different Mach numbers ($M_{\infty,i}$). The sum of the k drags coefficients is minimized. Figure 2 shows Huyse's results for two different multipoint optimizations. They observed that the multipoint approach leads to airfoils with k small bumps on the suction side, placed at the foot of the shocks for each of the k Mach numbers. The multipoint formulation found airfoils with better performance over the given set of Mach numbers, but they still exhibit unsatisfactory performance over the entire Mach range. To remedy the wavy behavior of the C_d *vs* Mach curves (see Figs. 1 and 2), Huyse et al. [3] proposed a formulation of the optimization problem that combines the multipoint formulation with a statistical approach to achieve a consistent drag reduction. Li et al. [6–8] have proposed robust optimization schemes and applied them to 2-D Euler flows and fully turbulent Navier–Stokes flows. They obtained relatively smooth shapes with no degradation in off-design performance over the range of Mach numbers. A common ground between the aforementioned studies is the use of splines or B-splines with a relatively large number of control points that can lead to bumpy airfoils when optimized for a single Mach number.

The present work explores further the topic of drag reduction by focusing on the effects of the geometric parameterization. We demonstrate that a NURBS parameterization yields smooth airfoils that do not exhibit severe performance degradation at off-design conditions. This assertion is based on previous work by Lépine et al. [9], which showed that NURBS constitute an effective means of accurately representing various existing airfoils. Furthermore, we perform optimization based on a high-fidelity Navier–Stokes solver, which can capture all the physics contributing to drag.

IV. NURBS Parameterization of Airfoils

A NURBS is defined in parametric form by

$$\boldsymbol{C}(u) = \sum_{i=0}^{n} R_{i,p}(u)\boldsymbol{P}_i$$

with

$$R_{i,p}(u) = \frac{N_{i,p}(u)\omega_i}{\sum_{j=0}^{n} N_{j,p}(u)\omega_j}$$

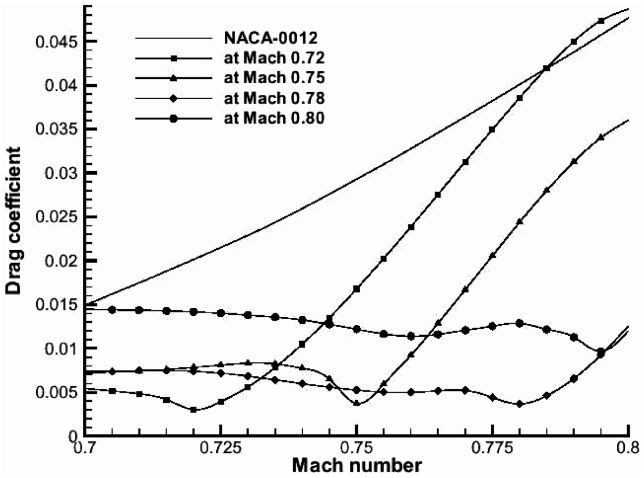

Fig. 1 C_d vs Mach for single-point optimizations using various design Mach numbers $C_l^* = 0.6$ (from Huyse et al. [3]).

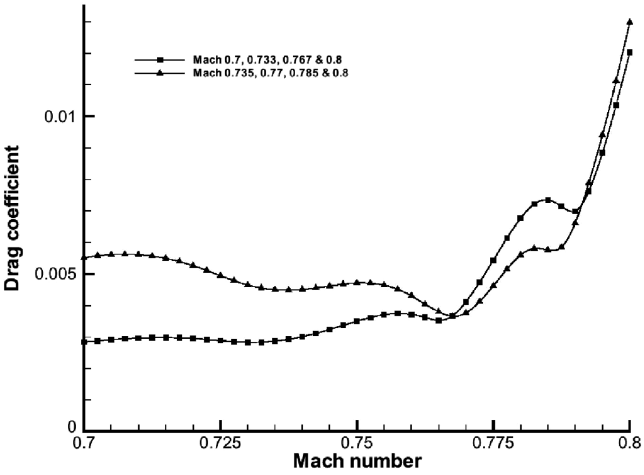

Fig. 2 C_d vs Mach for multipoint optimizations using various design Mach numbers $C_l^* = 0.6$ (from Huyse et al. [3]).

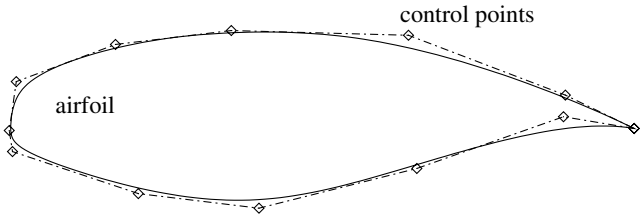

Fig. 3 Representation of a transonic airfoil using 13 control points.

where the $\boldsymbol{P}_i$ are the control points (see Fig. 3), ω_i their associated weights, $N_{i,p}$ the pth degree B-spline basis function and $\boldsymbol{C}(u)$ a vector-valued function returning the position of a point on the curve for a given value of the parameter u. For more details about the NURBS, their properties and the way they are obtained, please refer to Piegl and Tiller [10].

Using a NURBS parameterization ensures regularity properties of the airfoil geometric representation. The higher the order of the basis functions, the higher the order of the continuity. We have considered basis functions of degree 3 (order 4) such that the curves are at least C^2 continuous everywhere except at the end points.

The efficiency of NURBS for representing airfoil shapes and their applicability to shape optimization have been discussed by Lépine et al. [9,11]. NURBS provide an accurate representation of a wide variety of airfoils (RAE2822, Boeing A4, Boeing A8, Bombardier–Canadair, etc.) with 13 control points or less. (Lépine et al. [9,11] considered that a satisfactory representation of the original airfoil is obtained when the error of representation complies with

manufacturing tolerance and when the flow solver is insensitive to the error of representation.) For example, ten NURBS control points are sufficient to represent accurately the NACA0012 airfoil, whereas a typical transonic airfoil, such as those considered in the present work, requires 13 control points (see Fig. 3).

The NURBS representation introduces the possibility of changing the weights to control how the shape is attracted toward the control point polygon. With the same number of design parameters available, B-spline and NURBS do not have the same number of control points. A sufficiently large number of design parameters is required to represent complex airfoils shape by B-splines. However, the down side for adding more control points is that shape modifications occur at a smaller scale, which leads to bumpy airfoils: an undesirable effect. Thus, NURBS are an interesting alternative to splines and B-splines for aerodynamic optimization due to the increased smoothness of the airfoils parametrization.

V. Flow Solver and Grid Convergence

A Navier–Stokes flow solver is used for the evaluations of C_l and C_d because of the importance of viscous effects in the transonic regime. The CFD code selected is NSU2D [12], an unstructured mesh compressible Reynolds-averaged Navier–Stokes solver that computes steady-state flow in transonic and subsonic regimes over single and multielements airfoils. Each analysis took approximately 5 min on a 400 MHz SGI Origin2000.

Grid density influences both the accuracy of the solution obtained from the solver and the computation time. Thus, we seek a grid that yields satisfactory accuracy for the lowest possible computation time. NSU2D uses iterative steps, or cycles, to converge the solution. Thus, the number of cycles used is also a parameter affecting both the quality of the solution and the computing time. A rigorous grid convergence study has been carried out to find an acceptable compromise in terms of grid resolution and the number of iterative cycles. It has been found that a grid with 25,000 elements combined with 150 multigrid cycles provides an acceptable compromise between accuracy and CPU time. When compared with converged solution on a much finer grid, the combination of a 25000 elements grid and 150 cycles provides C_l to better than 10% and C_d to better than 5%. This combination has been used in the present optimization process to limit computation time. The solution obtained with this grid is subjected to noise with an amplitude of approximately 1.E-3 for both C_d and C_l (see Fig. 4). From a practical point of view, only shape modifications of the airfoil corresponding to C_l and C_d variations larger than the noise amplitude are considered as significant for optimization. Because of the range of possible improvements, the presence of noise and inaccuracies should not affect our conclusion regarding the ability of the method to produce good airfoils.

A limiting characteristic of NSU2D is that it cannot provide sensitivity informations and the gradients required for optimization must be evaluated by finite differences of the objective and constraint functions. This is extremely time consuming unless one can distribute the gradient calculation over a large number of CPU nodes, which was not possible during this study due to limited computer resources. More efficient approaches for evaluating gradients such as adjoint-based CFD codes should be considered for practical industrial applications.

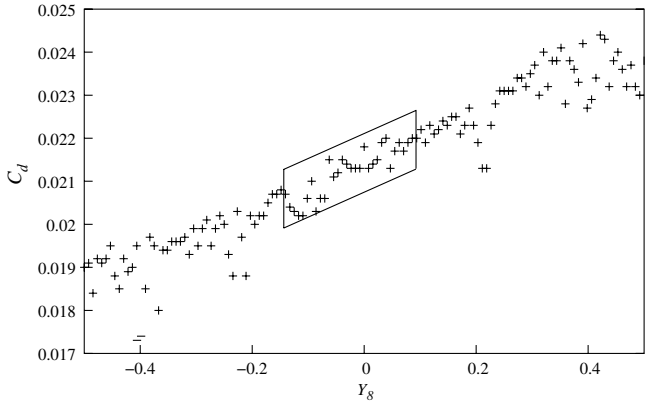

Fig. 4 Variations of C_d due to numerical noise.

VI. Airfoil Shape Optimization

A general mathematical statement of the airfoil shape optimization problem is given as follows:

$$\min_{\boldsymbol{d}} F(\boldsymbol{d})$$

$$\text{subject to } \boldsymbol{g}(\boldsymbol{d}) \geq 0$$

In cases where F and $\boldsymbol{g}$ are differentiable functions, this problem is efficiently solved by a sequential quadratic programming (SQP) algorithm [13,14]. In the present work, we selected the DONLP algorithm, available under the iSIGHT 7.0 environment, a product from Engineous Software.[‖] Such gradient-based methods have been used widely and are known for their efficiency. However, one must keep in mind that the optimum obtained by SQP methods will be a global optimum only if the objective and constraints are differentiable and convex functions. Typical aerodynamic objectives functions and constraints are not necessarily smooth or convex functions [15]. As a result, only a local optimum in the neighborhood of the initial point can usually be obtained. Preliminary optimization tests started from a NACA0012 airfoil have shown that the optimized airfoils possess shapes that are relatively close to the initial one and are far from those characteristic of supercritical airfoils. This is typical of gradient-based aerodynamic optimizations: the optimizer will usually find one of the many local extremum points caused by the complexity of the design space. Thus different initial shapes will likely produce different final design. Only global optimization algorithms can find radically new families of airfoils. However, global optimizers are generally very CPU intensive, which make them unsuitable for complex design problems unless they are combined with response surface approximations. This line of research constitutes one of the avenues explored by the multidisciplinary design optimization (MDO) community, but this is beyond the scope of the present paper. In an engineering design setting, using gradient-based methods can be justified in a more practical way: when aerodynamic optimizations are conducted on airfoils by aircraft manufacturers, the objective is often to improve an existing airfoil that is already efficient. Indeed, an improved design is sought near the initial airfoil and gradient-based methods are especially efficient at this task.

Having selected the type of optimization algorithm, several aspects of the optimization problem definition are critical: the selection and scaling of the design variables, the gradient computation and the definition of the objective function and constraints. These aspects will be reviewed in the next subsections.

A. Selection of the Design Variables

The initial transonic airfoil is represented with 13 control points, two being fixed at the trailing edge. Each of the 11 free control points $\boldsymbol{P_i}$ has 3 associated design parameters, x, y, and ω, leading to possibly 33 design variables in the optimization process. The angle of incidence of the flow is considered as an additional design variable (34 total) because it influences the aerodynamic performance of the profiles.

The SQP method requires gradient evaluation of the functions at each iteration of the optimizer, and because finite difference is used for gradient evaluations, the computation time is dominated by the gradient computations and is proportional to the number of design variables. To limit computation time, a reduction of the number of design variables is sought.

To guide our effort, a design of experiment (DOE) is performed at $M_\infty = 0.73$, which corresponds to the middle of the Mach range

[‖]For details, see http://www.engineous.com [cited 28 August 2006].

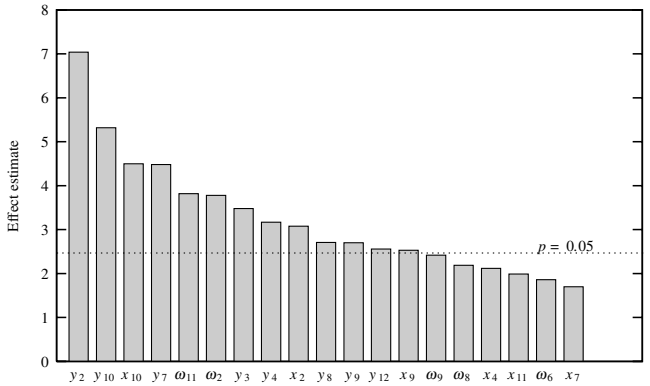

Fig. 5 Pareto diagram: estimated effects of each design variable on F_{DOE}.

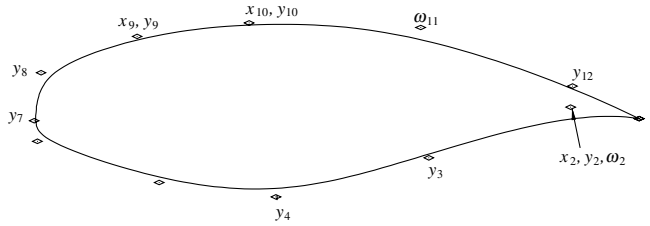

Fig. 6 Initial airfoil profile and design variables selected with the design of experiment (DOE).

studied in the present work. The x coordinate of the control points near the leading edge are kept constant for solver stability, leading to 30 design variables investigated. A design of experiment based on a 64 run plan obtained from Statistica has been performed.¶. Each design variable can take only its boundary values in the design space (see Sec. VI.B). To estimate the effect of the variables on the design quality, the following merit function has been used: $F_{\mathrm{DOE}} = C_l^{\mathrm{init}} C_d^2 / C_d^{\mathrm{init}} + (C_l - C_l^{\mathrm{init}})^2$.

The 13 most sensitive variables identified by a statistical analysis of the DOE runs (see the Pareto diagram on Fig. 5 used for the screening), have been selected as design variables and are shown on Fig. 6. In this study, screening of the design variables is performed once prior to the optimizations. A more comprehensive optimization strategy for the complete set of control points could include successive screenings of the sensitive design variables followed by optimization. The development of such strategy is beyond the scope of the current paper.

B. Scaling of the Design Variables

In general, for gradient-based methods, it is desirable that all the design variables be of the same order of magnitude. Large differences in the magnitude of variables results in ill conditioning of Hessians or Jacobian matrices, making calculations unstable [16]. Good scaling can be achieved with the use of dimensionless variables in the range $[-1, 1]$.

The optimizer handles the scaled variables without any knowledge about the nature of the problem and the variables. Thus, it is important that the scaling is such that similar changes in the design variables have similar effects to the airfoil shape. After experimentation, scaling is chosen so that a variation of the scaled variables between ± 1 yields an equivalent $\pm 5\%$ variation of the chord of the airfoil (c) for the x variables and $\pm 5\%$ variation of the maximum thickness of the initial airfoil ($t^*_{\max}$) for the y variables:

$$Y_i = \frac{\left(y_i - y_i^o\right)}{0.05 t^*_{\max}} \qquad X_i = \frac{\left(x_i - x_i^o\right)}{0.05 c}$$

¶A software from Statsoft, Inc. For details, see www.statsoft.com [cited 28 August 2006].

The initial airfoil considered for this study has a unit chord length ($c = 1$) and $t^*_{\max} = 0.12$. The scaling for the x variables is therefore:

$$X_i = 20\left(x_i - x_i^o\right)$$

After rounding down, the scaling for the y variables is the following:

$$Y_i = 150\left(y_i - y_i^o\right)$$

The weights affect the curve in a nonlinear way. When ω_i increases, the curve is pulled toward the point $\boldsymbol{P_i}$. Also, when $\omega_i = 0$, the position of $\boldsymbol{P_i}$ has no influence on the curve [10]. Based on this property, we have estimated that the influence of ω_i on the maximum thickness of the airfoil is better captured by a logarithmic representation than a linear one. Thus, the proposed scaling is the following:

$$\Omega_i = \frac{1}{\ell n(2)} \ell n\left(\frac{\omega_i}{\omega_i^o}\right)$$

This scaling ensures that for $\Omega_i = -1$ and $\Omega_i = 1$, the corresponding values of ω_i will be, respectively, $\omega_i = 0.5\omega_i^o$ and $\omega_i = 2\omega_i^o$, which correspond approximately to a $\pm 5\%$ variation of the maximum thickness of the initial airfoil.

The design vector for this study consists of $\boldsymbol{d} = \{X_2, X_9, X_{10}, Y_2, Y_3, Y_4, Y_7, Y_8, Y_9, Y_{10}, Y_{12}, \Omega_2, \Omega_{11}\}$ and α.

C. Determination of the Differentiation Step Size

SQP optimizers first determine a desired search direction that minimizes a quadratic approximation of the objective function subject to linear approximations of the constraints. All approximations require derivatives with respect to each design variable. The evaluations of the gradient of F and $\boldsymbol{g}$ are thus critical for finding a good search direction. In the SQP method used, the derivatives are approximated using a forward finite difference:

$$\frac{\partial F}{\partial d_i} \approx \frac{F(d_i + h) - F(d_i)}{h}$$

where h is the differentiation step size specified by the user. The step size must be chosen very carefully to ensure the accuracy of the gradients, especially when noisy functions are differentiated. Larger step sizes provide gradients that are less affected by numerical noise, but they also cause losses in gradients accuracy due to truncation error. We implemented a successive step size reduction strategy in our optimization process: a coarse step size is used at first to help the optimizer explore larger zones of the design space and to help overcome local minima of the function F. The newly found airfoil is used as a new initial guess of the airfoil shape, and then a finer step size is used (half of the previous one) in a new optimization process. The finer step size allows the optimizer to explore more locally around the newly found airfoil. The process is repeated until the step size reaches the order of the numerical noise, which has been determined beforehand by a sensitivity analysis [17].

D. Separation of the Optimization Problem

The original single-point formulation of the drag minimization problem is the following:

$$\begin{aligned} &\min_{\alpha, \boldsymbol{d}} C_d(\boldsymbol{d}, \alpha, M_\infty) \\ &\text{s.t.: } C_l(\boldsymbol{d}, \alpha, M_\infty) \geq C_l^* \\ &t_{\max}(\boldsymbol{d}) \geq t^*_{\max} \end{aligned} \tag{1}$$

In the present work, the maximum thickness of the airfoil is controlled by introducing an explicit constraint in the formulation of the optimization problem: $t_{\max}(\boldsymbol{d}) \geq t^*_{\max}$ where $t^*_{\max}$ is the maximum thickness of the initial airfoil. This is a simple way of representing the wing box structure volume requirements.

Table 1 C_d at different M_∞ for the initial and the single-point optimized airfoils

	$M_\infty = 0.705$		$M_\infty = 0.73$		$M_\infty = 0.755$	
Design	C_d	Gain	C_d	Gain	C_d	Gain
Initial airfoil	0.0134	——	0.0213	——	0.0746	——
Single-point ($M_{\infty,1} = 0.705$)	0.0102	23.9%	0.0189	11.3%	0.0641	14.1%
Single-point ($M_{\infty,2} = 0.73$)	0.0119	11.2%	0.0107	49.8%	0.0282	62.2%
Single-point ($M_{\infty,3} = 0.755$)	0.0186	−38.8%	0.0147	31.0%	0.0174	76.7%

In the NSU2D flow solver used to compute C_d and C_l, α is the angle of the upstream flow with respect to the horizontal x axis. This is to be distinguished from the usual definition of the angle of attack. Obviously, the angle α does not influence the shape of the airfoil, however, the angle of attack of the airfoil relative to the flow field depends slightly on the design variables $\boldsymbol{d}$.** To clarify the role of each design variable, we have implemented a procedure to rescale and rotate the airfoil such that, independently of $\boldsymbol{d}$, the chord segment lies between (1,0) and (0,0); that is, the airfoil always has a unit chord length. Thus, by using this procedure, α and the usual angle of attack become identical, and the angle of attack of the rescaled airfoil is independent of $\boldsymbol{d}$.

Note that, by its nature α can be considered separately from the geometric variables $\boldsymbol{d}$. By fixing the design vector $\boldsymbol{d}$, the original formulation becomes an optimization subproblem, which is written as follows:

$$\min_{\alpha} C_d(\boldsymbol{d}, \alpha, M_\infty)$$
$$\text{s.t.: } C_l(\boldsymbol{d}, \alpha, M_\infty) \geq C_l^*$$

With our rescaling and rotation, α is not affected by the geometric constraints which are removed from the subproblem. Moreover, for the vast majority of nonstalled airfoils, increasing α leads to larger values of C_l and C_d. Therefore, finding α so that C_l is as close as possible to C_l^* will ensure that C_d is minimized for a given airfoil while satisfying the lift constraint. Thus, we consider the following new optimization subproblem:

$$\min_{\alpha} \alpha$$
$$\text{s.t.: } C_l(\boldsymbol{d}, \alpha, M_\infty) \geq C_l^* \tag{2}$$

The optimal value returned by the subproblem is noted α^+.

The master problem is now rewritten as

$$\min_{\boldsymbol{d}} C_d(\boldsymbol{d}, \alpha^+, M_\infty)$$
$$\text{s.t.: } t_{\max}(\boldsymbol{d}) \geq t_{\max}^* \tag{3}$$

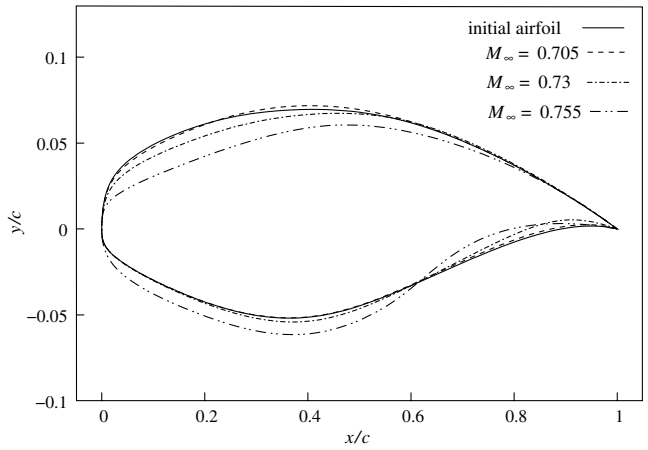

Fig. 7 Initial transonic airfoil and single-point optimized airfoils at $M_\infty = 0.705$, $M_\infty = 0.73$, and $M_\infty = 0.755$.

**The angle of attack considered here is the angle between the chord of the airfoil and the upstream flow direction. The chord line connects the trailing edge and the point of the airfoil the most distant from the trailing edge, which in general depends on the shape of the airfoil.

The master optimizer works only on reducing the drag because the lift constraint is always satisfied via the suboptimization. Each evaluation of $C_d(\boldsymbol{d}, \alpha^+, M_\infty)$ requires the solution of the optimization subproblem given in formulation (2). This suboptimization requires on the average five or six calls to the flow solver for each evaluation of $C_d(\boldsymbol{d}, \alpha^+, M_\infty)$ needed by the master problem.

VII. Optimization Formulations and Results

A. Single-Point Optimization

Three single-point optimizations [using formulations (2) and (3)] have been performed separately for three flight conditions: $M_\infty = 0.705$, $M_\infty = 0.73$, and $M_\infty = 0.755$ at $Re = 1E6$. The constraints parameters are $C_l^* = 0.8$ and $t_{\max}^* = 0.12$, which correspond to the lift of the initial airfoil at $M_\infty = 0.73$ and $\alpha \approx 2.5$ deg, and to the maximum thickness of the initial airfoil.

Figure 7 illustrates the resulting optimized airfoils. In all cases, the three optimized airfoils are very smooth and the shock strength is reduced without introducing localized bumps on the upper surface of the airfoil. The optimizer was able to handle the thickness constraint because all optimized airfoils have a maximum thickness above $t_{\max}^* = 0.12$ ($t_{\max} = 0.1232$, 0.1203, 0.1200 for $M_\infty = 0.705$, $M_\infty = 0.73$, and $M_\infty = 0.755$, respectively). Also, the lift constraint $C_l > C_l^*$ is saturated, that is, $C_l = 0.7991$, 0.7997, and 0.7995, respectively. Notice that the difference between the optimal and the initial airfoils increases with Mach number. For the highest Mach number, the optimum exhibits the characteristics of supercritical airfoil: flat upper surface and accentuated curvature change on the lower surface [18].

Table 1 summarizes the results in term of the drag coefficient C_d. For the initial airfoil, the computed drag coefficient for the three flight conditions is given in the first line. One can observe a major increase in C_d at $M_\infty = 0.755$. In the same table, under each flight condition, two columns report the drag coefficient of the optimized airfoils and the gain in percentage with respect to the drag of the initial airfoil. Notice that the airfoil optimized with the single-point formulation at $M_\infty = 0.705$ provides the best gain at that condition. The same is true for the airfoils optimized at $M_\infty = 0.73$ and $M_\infty = 0.755$. Significant reduction in C_d is observed at $M_\infty = 0.755$, that is a gain of 76.7% over the performance of the initial airfoil at the same condition.

Thanks to the use of the Navier–Stokes flow solver, the optimizer was clearly able to capture the shock wave/boundary layer interaction to minimize drag at constant lift. Figures 8a and 8b illustrate how the shocks are reduced after optimization at $M_\infty = 0.705$ and $M_\infty = 0.73$. For these two flight conditions, the gains in C_d are 23.9 and 49.8%, respectively. These constitute significant improvements given that the initial airfoil is already well adapted to the transonic regime. Figures 9a and 9b, show that the boundary layer remains attached through the optimization. Note also that because the friction drag is slightly increased by the optimization, the gain in total drag is mainly due to the reduction of wave drag.

The C_p curve at $M_\infty = 0.755$ [see Fig. 8c] shows that the shock has been moved downstream by the optimization process, whereas the amplitude of the shock remained unchanged. Also, as discussed previously, the gain in C_d for this flight condition is 76.7%, mainly due to the reduction of form drag. In fact, as can be seen on Fig. 9c, the boundary layer on the upper surface before optimization was separated, resulting in a negative friction coefficient downstream of $x/c = 0.4$, and high form drag. After optimization, the boundary layer is attached on both the upper and lower surfaces, resulting in

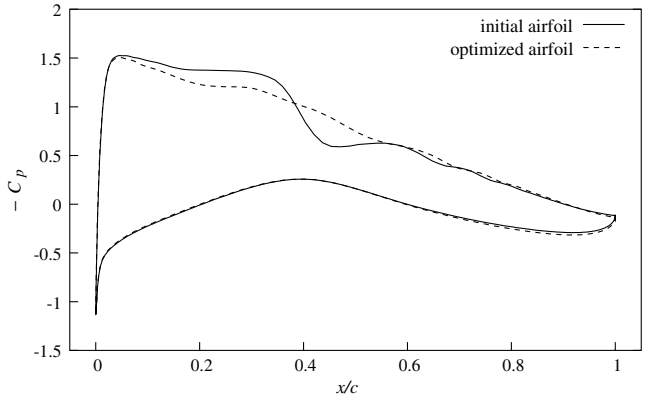

a) $M_\infty = 0.705$

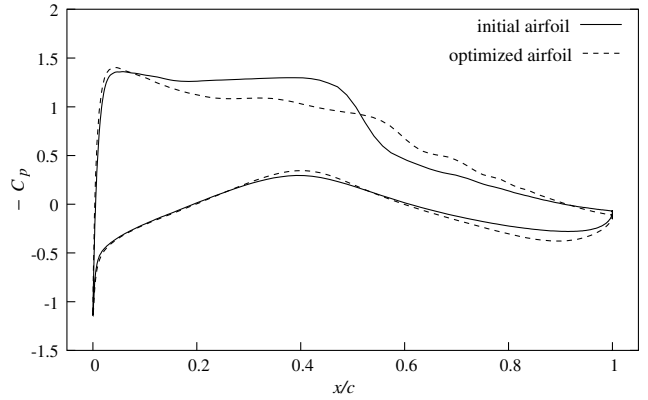

b) $M_\infty = 0.73$

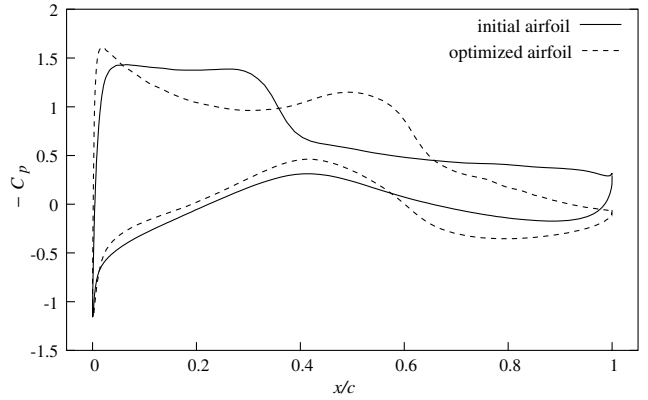

c) $M_\infty = 0.755$

Fig. 8 C_p curves for the initial airfoil and the single-point optimized airfoil at various Mach numbers.

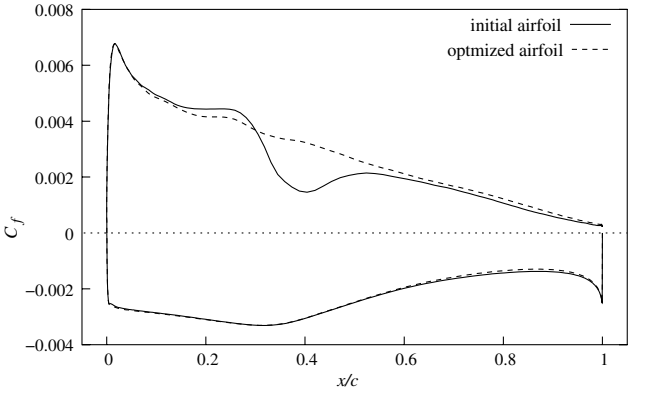

a) $M_\infty = 0.705$

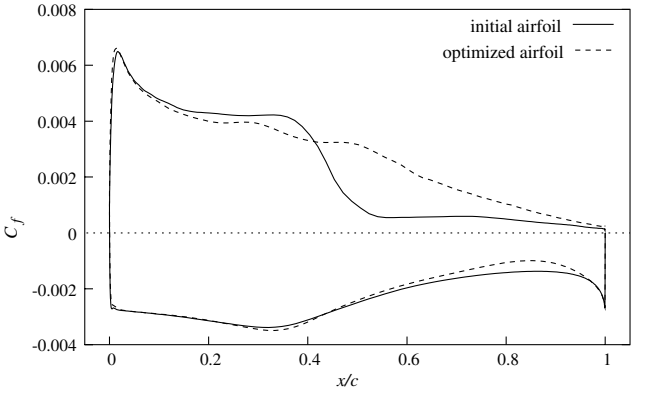

b) $M_\infty = 0.73$

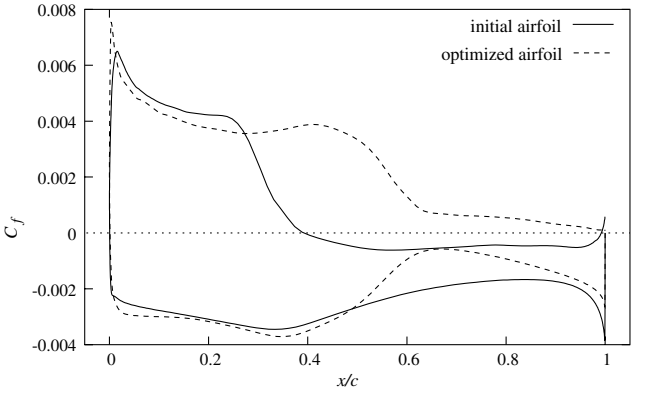

c) $M_\infty = 0.755$

Fig. 9 C_f curves for the initial airfoil and the single-point optimized airfoil at various Mach numbers.

lower form drag. For this case, the optimizer "senses" the boundary layer effects on the total drag coefficient. One can also observe on Fig. 9c that friction drag increases during optimization. Thus, the Navier–Stokes flow solver helps to find designs that are well suited to flight conditions where form drag is the dominant component of total drag, due to the interaction between the shock wave and boundary layer.

Figure 10 presents the drag-rise curves at constant C_l for the three optimized airfoils. They are obtained by CFD analyses (unchanged grid refinement) of the optimized shapes by varying α to ensure that $C_l = C_l^* \pm 0.0008$ at each Mach number. One can see that the drag coefficient C_d is slightly increased at off-design conditions. A "mild" local minimum of C_d is found at the design point of each of the three optimized airfoils. However, the localized effects are much less pronounced than those observed in past work on the subject (see Fig. 1).

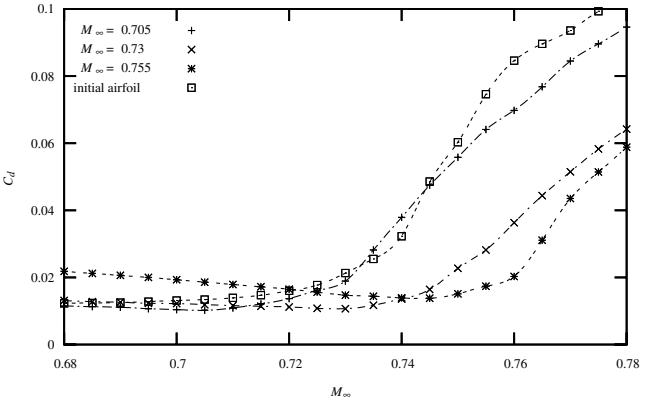

Fig. 10 C_d *vs* M_∞ for single-point optimized airfoils, $C_l = C_l^* = 0.8$.

Table 2 C_d at different M_∞ for the initial and the optimized airfoils

	$M_\infty = 0.705$		$M_\infty = 0.73$		$M_\infty = 0.755$		$M_\infty = 0.705, 0.73, 0.755$	
Design	C_d	Gain	C_d	Gain	C_d	Gain	F_{comp}	Gain
Initial airfoil	0.0134	——	0.0213	——	0.0746	——	1	——
Single-point ($M_{\infty,1} = 0.705$)	0.0102	23.9%	0.0189	11.3%	0.0641	14.1%	0.836	16.4%
Single-point ($M_{\infty,2} = 0.73$)	0.0119	11.2%	0.0107	49.8%	0.0282	62.2%	0.589	41.1%
Single-point ($M_{\infty,3} = 0.755$)	0.0186	−38.8%	0.0147	31.0%	**0.174**	**76.7%**	0.775	22.5%
Multipoint	**0.0101**	**24.6%**	**0.0105**	**50.7%**	0.0202	72.9%	**0.505**	**49.5%**

B. Multipoint Optimization

Although the three airfoils obtained with single-point optimizations were all smooth and optimal for their respective design Mach number, their final shape was dependent on the operating Mach number and their drag-rise behavior was not flat over a Mach range. To find an airfoil with good performance for a given Mach range, one must consider multipoint optimization.

In practice, CFD provides information for a set of discrete values of the Mach number. Hence, one must select a few flight conditions spanning the entire range. Because the tradeoff between the various flight conditions can be expressed as a multiobjective optimization problem, or vector-optimization problem, there is in general no single global solution to such a problem. For example, depending on the importance given to each flight condition, the optimal design obtained can be different.

In the present case, the importance of each flight condition is considered to be known in advance, all objectives having the same nature and a common measure. In such a case, it is advantageous to transform the original vector-valued objective function into a scalar one defining which compromise should be made. The idea is to create a scalar objective function out of the vector objective function. First, each objective is normalized by its initial value. Second, a scalar objective function is defined by summing all the individual objectives. The preference given to each individual objective is reflected by the value given to its weighting factor in the summation. The compromise objective function is written as

$$F_{\text{comp}} = \sum_{i=1}^{k} w_i \left[\frac{C_{d,i}(\boldsymbol{d}, \alpha_i, M_{\infty,i})}{C^o_{d,i}} \right] \tag{4}$$

Using the compromise objective leads to the following multipoint formulation for the airfoil shape optimization problem:

$$\min_{\boldsymbol{d}} \sum_{i=1}^{k} w_i \left[\frac{C_{d,i}\left(\boldsymbol{d}, \alpha_i^+, M_{\infty,i}\right)}{C^o_{d,i}} \right] \quad \text{s.t.: } t_{\max}(\boldsymbol{d}) \geq t^*_{\max} \tag{5}$$

subject to the k optimization subproblems:

$$\alpha_i^+ = \min_{\alpha_i} \alpha_i \quad \text{s.t.: } C_l(\boldsymbol{d}, \alpha_i, M_{\infty,i}) \geq C^*_l \tag{6}$$

This formulation has been applied with the same constraints used in the single-point formulation, that is, $C^*_l = 0.8$ and $t^*_{\max} = 0.12$. The three flight conditions (i.e., $M_{\infty,1} = 0.705$, $M_{\infty,2} = 0.73$, and $M_{\infty,3} = 0.755$, with $Re = 1\text{E}6$) are weighted equally ($w_i = \frac{1}{3}$). This can be interpreted as meaning that the airfoil operates at each M_∞ for an equal fraction of the flight time. This condition has been chosen because it corresponds to a worst case scenario, making the optimization process even harder. In a more practical case, if the design point of the airfoil were, say, $M_\infty = 0.73$, we could choose the same $M_{\infty,i}$ with weights based on a normal distribution of the flight conditions as discussed by Huyse et al. [3]. The number of flight conditions can also be changed, but a higher number always leads to a longer optimization because every airfoil generated must be analyzed at each of the k values in the set of flight Mach numbers.

Figure 11 depicts the airfoil resulting from the multipoint optimization. It is as smooth as the initial airfoil. The upper surface has been flattened and the curvature change on the lower surface has been accentuated.

Table 2 summarizes the results obtained by the single-point and the multipoint formulations. As expected, in terms of the compromise objective function F_{comp} [see Eq. (4)], the multipoint-optimized airfoil performs better than any of the single-point optimized airfoil: the gain is 49.5% with the multipoint formulation (emphasized number in the right column of the table) compared with 16.4%, 41.1%, and 22.5% for the single-point formulation at $M_\infty = 0.705$, $M_\infty = 0.73$, and $M_\infty = 0.755$, respectively. Thus, the multipoint approach produces an airfoil with better performance over the Mach range than any airfoil obtained with the single-point formulation. Figure 12 shows a comparison of the drag-rise curves resulting from the single-point and the multipoint formulations. Notice that localized effects, observed with the single-point optimizations, have disappeared from the C_d *vs* M_∞ curve thank to the multipoint formulation. Notice also that the drag-rise curve of the multipoint-optimized airfoil is very flat.

However, a surprising result is observed when comparing values of C_d obtained with the different formulations. Table 2

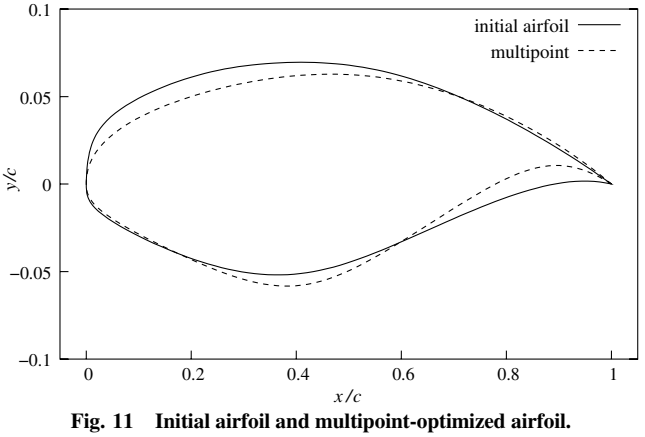

Fig. 11 Initial airfoil and multipoint-optimized airfoil.

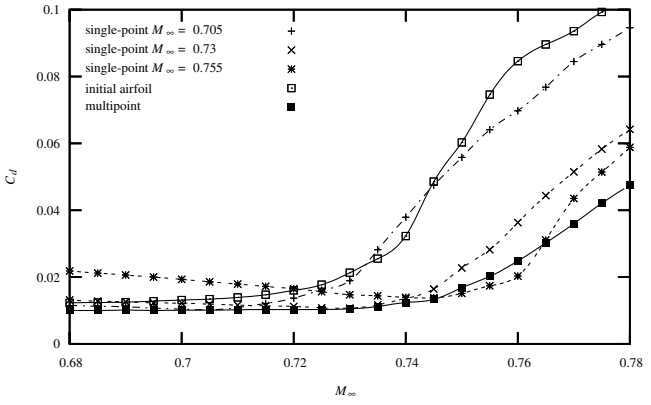

Fig. 12 C_d vs M_∞ for the multipoint and single-point optimized airfoils, $C_l = C^*_l = 0.8$.

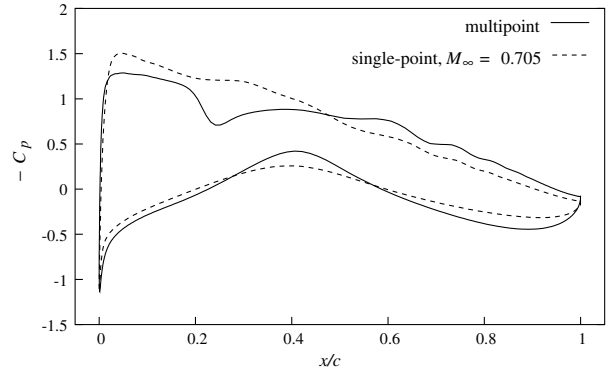

a) $M_\infty = 0.705$

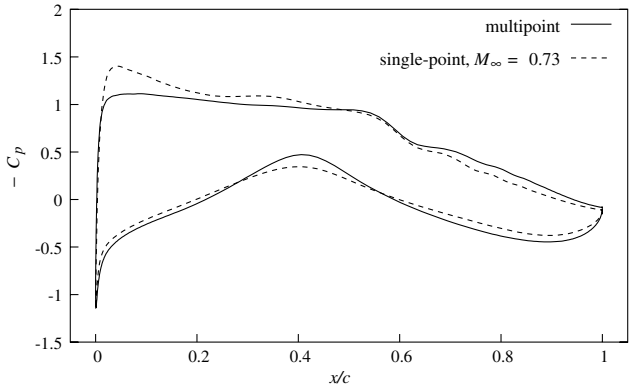

b) $M_\infty = 0.73$

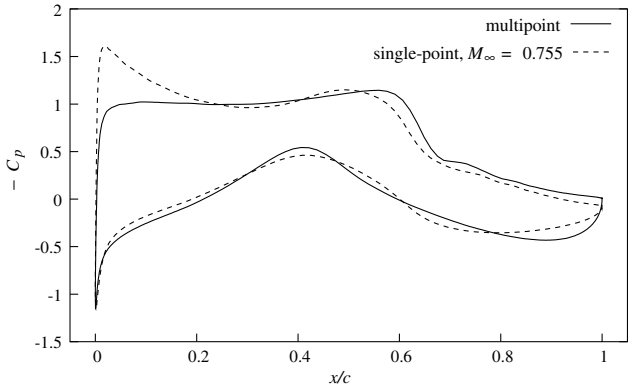

c) $M_\infty = 0.755$

Fig. 13 C_p curves for the initial airfoil and the multipoint-optimized airfoil at various Mach numbers.

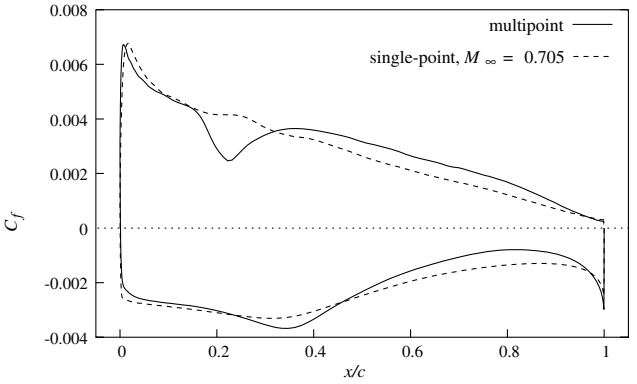

a) $M_\infty = 0.705$

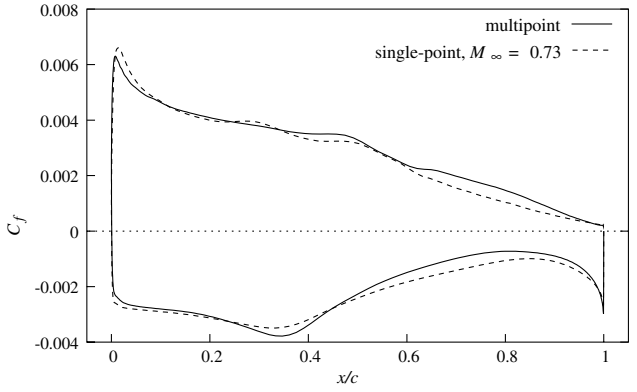

b) $M_\infty = 0.73$

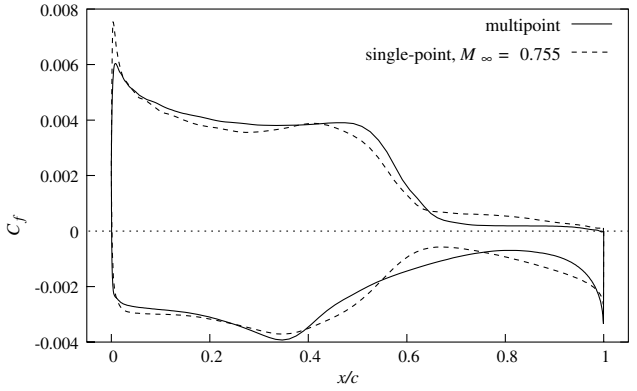

c) $M_\infty = 0.755$

Fig. 14 C_f curves for the initial airfoil and the multipoint-optimized airfoil at various Mach numbers.

shows that the multipoint-optimized airfoil performs slightly better at $M_\infty = 0.705$ and $M_\infty = 0.73$ than the single-point optimized airfoils at the same Mach number. The difference is marginal at $M_\infty = 0.705$, with $C_d = 0.0101$ using the multipoint formulation and $C_d = 0.0102$ using the single-point one. Approximately the same difference is observed at $M_\infty = 0.73$. However, the trend is reversed at $M_\infty = 0.755$, where the single-point optimized airfoil performs better than the multipoint-optimized airfoil. This behavior can be explained by the fact that the single-point optimization may get caught in a local minimum for one Mach number whereas the multipoint optimization has lead to a more global optimal solution.

C_p curves on Fig. 13a show that a weak shock is present for the multipoint-optimized airfoil at $M_\infty = 0.705$ whereas it is absent with the single-point optimized airfoil. On Figs. 13b and 13c, it is interesting to note that the C_p curves obtained by multipoint optimization are typical of supercritical airfoils with large constant pressure plateaux on the upper surface. As for the friction coefficient, the curves are rather similar to those obtained with single-point optimizations [see Figs. 14a–14c].

Optimization history for the different formulations is illustrated on Fig. 15 in terms of objective function improvements *vs* master problem iteration. One master problem iteration requires an average of 85 solver calls for each Mach number. For the single-point formulation, the higher the Mach number, the larger the number of iterations required to converge. In fact, the optimizer experiences difficulties in reducing wave drag. Obviously, the multipoint formulation combines all the difficulties of the single-point optimization in addition to finding a good compromise between all the regimes. These additional difficulties result in slower convergence.

VIII. Conclusion

In this work, we have shown that a NURBS parameterization helps produce smooth airfoils for drag minimization problems. This is

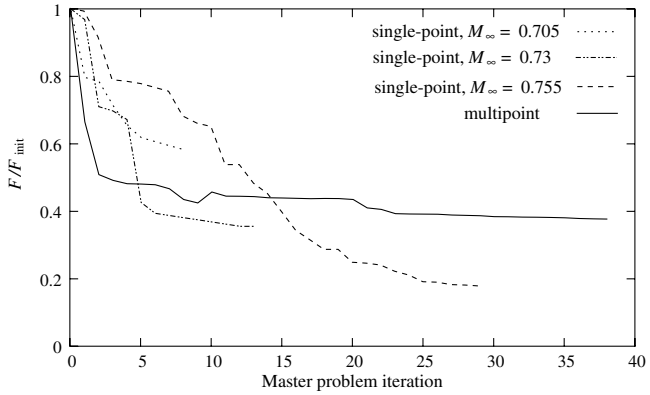

Fig. 15 Optimizations history.

important as NURBS are often the parameterization of choice in many CAD systems.

First, a design of experiment was conducted to select the most sensitive design variables and reduce their number. An explicit constraint on the maximum relative thickness has been implemented to obtain realistic airfoils.

A bilevel formulation of the optimization problem has been proposed in which the design variables are split in two groups, each one having a specific goal. In the main problem, the design variables are the position of NURBS control points determining the geometry of the airfoil, and the objective is total drag reduction. In the subproblem, the design variable is the angle of attack and the objective is to satisfy the lift constraint for the smallest possible angle of attack.

A Navier–Stokes flow solver has been used to account for both wave drag and drag due to shock/boundary layer interaction.

Because the NURBS parameterization leads to fewer design parameters, the risk of introducing bumps in the shape of the airfoil is significantly reduced. This eases the aerodynamic optimization process because the NURBS representation of the airfoil is naturally constrained to have good regularity properties. Also, the small number of design variables results in tractable optimization problems. With the single-point formulation, NURBS provide airfoils with mild aerodynamic changes at off-design flight conditions. However, as can be expected, the single-point optimized airfoil shows some Mach number dependency and their corresponding C_d *vs* M_∞ curves present a mild minimum at the Mach number for which the airfoil has been optimized. The proposed multipoint formulation, which uses three different Mach number equally spaced in the intended Mach range, prevents this behavior. The resulting optimized airfoil is smooth and presents good performance over the specified range of flight conditions.

Acknowledgments

This work was supported in part by the Natural Sciences and Engineering Research Council (Canada), Fonds Québécois de la Recherche sur la Nature et la Technologie (Québec), and the Canada Research Chair Program (Canada). The authors would like to thanks François Pépin and David Leblond from Bombardier Aerospace for fruitful discussions on airfoil aerodynamic design.

References

[1] Lores, M. E., and Hinson, B. L., "Transonic Design Using Computational Aerodynamics," *Transonic Aerodynamics*, Vol. 81, Progress in Astronautics and Aeronautics, Chap. VII, American Institute of Aeronautics and Astronautics, Inc., Reston, VA, 1982, pp. 377–402.

[2] Drela, M., "Pros and Cons of Airfoil Optimization," *Frontiers of Computational Fluid Dynamics*, edited by D. Caughey and M. Hafez, World Scientific, Singapore, 1998, pp. 363–381.

[3] Huyse, L., Padula, S. L., Lewis, R. M., and Li, W., "Probabilistic Approach to Free-Form Airfoil Shape Optimization Under Uncertainty," *AIAA Journal*, Vol. 40, No. 9, 2002, pp. 1764–1772.

[4] Tribes, C., and Trépanier, J.-Y., "Airfoil Shape Optimization," *Proceedings of the International Conference on Multidisciplinary Design in Engineering, CSME-MDE 2001*, University Concordia, Montréal, Canada, 2001.

[5] Anderson, J. D., Jr., *Modern Compressible Flow*, 2nd ed., McGraw–Hill Publishing Company, New York, 1990.

[6] Li, W., Huyse, L., and Padula, S., "Robust Airfoil Optimization to Achieve Drag Reduction over a Range of Mach Numbers," *Structural and Multidisciplinary Optimization*, Vol. 24, No. 1, 2002, pp. 38–50.

[7] Li, W., and Padula, S., "Performance Trades Study for Robust Airfoil Shape Optimization," AIAA Paper No. AIAA-2003–3790, 2003, pp. 1–7.

[8] Li, W., and Padula, S., "Using High Resolution Design Spaces for Aerodynamic Shape Optimization Under Uncertainty," NASA Langley Research Center, Tech. Rept. NASA/TP-2004–213003, Hampton, Virginia, March 2004.

[9] Trépanier, J.-Y., Lépine, J., and Pépin, F., "An Optimized Geometric Representation for Wing Profiles Using NURBS," *Canadian Aeronautics and Space Journal (Le Journal Aeronautique et Spatial du Canada)*, Vol. 46, No. 2, March 2000, pp. 12–19.

[10] Piegl, L., and Tiller, W., *The NURBS Book*, Springer–Verlag, New York, 1995.

[11] Lépine, J., Guibault, F., Trépanier, J.-Y., and Pépin, F., "Optimized Non-Uniform Rational B-Spline Geometrical Representation for Aerodynamic Design of Wings," *AIAA Journal*, Vol. 39, No. 11, Nov. 2001, pp. 2033–2041.

[12] Mavriplis, D. J., *A CFD Package for Multi-Element Airfoil High-Lift Analysis*, Scientific Simulation, Yorktown, VA, Dec. 1996.

[13] Spelluci, P., "An SQP Method for General Nonlinear Programs Using only Equality Constrained Subproblems," *Mathematical Programming*, Vol. 82, No. 3, 1998, pp. 413–448.

[14] Vanderplaats, G. N., *Numerical Optimization Techniques for Engineering Design*, Vanderplaats Research & Development, Inc., Colorado Springs, CO, 1999.

[15] Takahashi, S., Obayashi, S., and Nakahashi, K., "Inverse Design Optimization of Transonic Wings Based on Multi-Objective Genetic Algorithms," *AIAA Journal*, Vol. 37, No. 12, Dec. 1999, pp. 1656–1662.

[16] Papalambros, P. Y., and Wilde, D. J., *Principles of Optimal Design*, Cambridge University Press, Cambridge, U.K., 2000.

[17] Painchaud-Ouellet, S., Optimisation Aérodynamique de Profils d'Aile 2-D, Master's Thesis, Département Génie Mécanique, École Polytechnique de Montréal, 2003.

[18] Lynch, F. T., "Commercial Transports: Aerodynamic Design for Cruise Performance Efficiency," *Transonic Aerodynamics*, Vol. 81, Progress in Astronautics and Aeronautics, Chap. II, American Institute of Aeronautics and Astronautics, Inc., Reston, VA, 1982, pp. 81–148.

A. Messac
Associate Editor